Phase-matching-free pulse retrieval based on transient absorption in solids

J.-C Delagnes, M R Bionta, F. Légaré, A. Leblanc, P. Lassonde, S. Petit, J.-C Delagn, E. Haddad, G Ernotte, V. Gruson, et al.

Research Article | Vol. 27, No. 20 / 30 September 2019 / Optics Express 28998
Optics EXPRESS

Phase-matching-free pulse retrieval based on transient absorption in solids

A. Leblanc,[1,2] P. Lassonde,[1] S. Petit,[2] J.-C. Delagnes,[2] E. Haddad,[1] G. Ernotte,[3] M. R. Bionta,[1] V. Gruson,[1] B. E. Schmidt,[1] H. Ibrahim,[1] E. Cormier,[2] and F. Légaré[1,*]

[1] *Institut National de la Recherche Scientifique, Centre EMT, ALLS laboratory, 1650 Boulevard Lionel-Boulet, Varennes, Quebec J3X1S2, Canada*
[2] *Centre National de la Recherche Scientifique, Centre Lasers Intenses et Applications, 351, Cours de la Libération, Talence, France*
[3] *Joint Attosecond Science Laboratory, National Research Council of Canada and University of Ottawa, Ottawa, Ontario K1A 0R6, Canada*
[*] *legare@emt.inrs.ca*

Abstract: In this paper, we introduce a pulse characterization technique that is free of phase-matching constraints, exploiting transient absorption in solids as an ultrafast optical switch. Based on a pump-probe setup, this technique uses pump pulses of sufficient intensity to induce the switch, while the pulses to characterize are probing the transmissivity drop of the photoexcited material. This enables the characterization of low-intensity ultra-broadband pulses at the detection limit of the spectrometer and within the transparency range of the solid. For example, by using zinc selenide (ZnSe), pulses with wavelengths from 0.5 to 20 μm can be characterized, denoting five octaves of spectral range. Using ptychography, we retrieve the temporal profiles of both the probe pulse and the switch. To demonstrate this approach, we measure ultrashort pulses from a titanium-sapphire (Ti-Sa) amplifier, which are compressed using a hollow core fiber setup, as well as infrared to mid-infrared pulses generated from an optical parametric amplifier (OPA). The characterized pulses are centered at wavelengths of 0.77, 1.53, 1.75, 4, and 10 μm, down to sub-two optical cycles duration, exceeding an octave of bandwidth, and with energy as low as a few nanojoules.

1. Introduction

With the advance of ultrafast laser technologies and nonlinear optics, ultrashort pulses from the UV to the mid-infrared are widely available [1–4]. Pulses over a broad spectral range are often simultaneously combined in pump-probe experiments. The characterization of such a variety of pulses requires different metrology techniques, depending on their specifications (i.e. energy, central wavelength, bandwidth). Moreover, cutting-edge technologies enable the generation of pulses with spectra exceeding one octave [5–7], which are even more challenging to characterize with conventional approaches.

For the complete characterization of ultrashort pulses, multiple techniques based on nonlinear optical (NLO) processes are exploited. For example, with self-referenced spectral interferometric techniques, the phase information is encoded in the interference pattern [8,9]. Other techniques use frequency conversion in order to couple the amplitude and phase of different frequencies contained in the optical pulses. This is the principle of frequency resolved optical gating (FROG) where an optical gate is created via a copy of the pulse [10], and of cross-correlation FROG (or X-FROG) where the gate is a second pulse [11]. In FROG, the spectral amplitude and phase of the pulses are encoded in the intensity of the recorded spectrogram consisting of spectra measured for various time delays between the two pulses. From the redundancy contained in the spectrogram, this technique allows the extraction of the pulse's temporal profile with advanced

#361498 https://doi.org/10.1364/OE.27.028998
Journal © 2019 Received 4 Mar 2019; revised 9 Aug 2019; accepted 11 Aug 2019; published 25 Sep 2019

Optics EXPRESS

algorithms. As a summary of more than two decades of intense research activities on pulse characterization, we suggest the following literature for review on this topic: [11,12].

Approaches based on frequency conversion have proven reliable in pulse reconstruction; however, the underlying nonlinear parametric interaction requires fulfillment of the phase matching condition. In the case of frequency conversion based techniques, such as second harmonic generation (SHG) FROG, this is the limiting factor for the addressable pulse bandwidth. For instance, measuring few-cycle pulses at 0.8 μm by SHG FROG requires a Beta Barium Borate (BBO) crystal of only a few-μm thickness. To circumvent this difficulty, the phase-matching condition can be greatly relaxed [13] by using third order nonlinearities such as transient grating and polarization gating FROG.

Over the recent years, NLO-based techniques have been refined and extended to enable the characterization of single and sub-cycle pulses [14,15]. For example, the trigger of sub-cycle tunnel ionization in air was used to characterize near single cycle pulses [16]. Furthermore, electro-optical sampling [17] has been extended to the near-IR region with the requirement of a sampling pulse which has a duration shorter than the optical cycle of the pulses to be characterized, which is required to be carrier-to-envelop phase stable for multi-shot measurements.

Here, we present an alternative pulse retrieval technique based on transient absorption in solids. The pulse to be characterized probes the ultrafast switch of the transient optical transmission of a solid triggered by a pump pulse. The switch originates from the photoexcited carrier dynamics and acts as a temporal knife-edge, slicing the probe pulse waveform whose transmitted spectrum is then recorded as a function of the pump-probe delay. From this spectrogram, we extract the temporal profiles of both the probe pulse and the switch using ptychographic algorithms. This approach does not rely on nonlinear frequency conversion, and therefore is neither limited by the phase matching constraint nor the intensity of the pulse (as long as they are above the noise floor of the detector). The pulses to be characterized are synchronized to pump pulses whose intensity is sufficient to induce the photoexcitation. This metrology is therefore well-suited to characterize the output pulses from optical parametric amplifiers, which are a key technology to extend the central frequency of ultrafast lasers to the infrared and mid-infrared spectral range.

Frequency resolved optical switching enables the characterization of ultra-broadband pulses at the detection limit of the spectrometer, and within the transparency range of the employed solid. To demonstrate the capability of this technique, we have characterized ultrashort pulses with central wavelengths from 0.77 to 10 μm, with a duration down to sub-two optical cycles, and energies down to few nanojoules.

2. Principle of frequency resolved optical switching

Using transient absorption in solids, well-known spatial ptychography can be transposed to the time-domain. Coming from microscopy, ptychography consists of measuring the pattern $I(\mathbf{k})$ of a probe $P(\mathbf{r})$ diffracted out on an object $O(\mathbf{r})$ for many relative positions $\mathbf{r}_0$. The measured 3D dataset is described by the following equation:

$$I(\mathbf{k}, \mathbf{r}_0) = \left| \int_{\mathbf{r}} P(\mathbf{r}) O(\mathbf{r} - \mathbf{r}_0) e^{i\mathbf{k}\mathbf{r}} \mathrm{d}\,\mathbf{r} \right|^2 . \tag{1}$$

Phase retrieval algorithms were developed to exploit the redundancy of information in the dataset to extract the spatial profiles of the probe and the object [18].

Here, transient absorption is described as a ptychographic experiment in the time-domain. This process creates an ultrafast switch $S(t)$ that is the temporal equivalent to the object in spatial ptychography. It is probed by the pulses to be characterized $P(t)$. As shown in Fig. 1, under our experimental conditions, by illuminating an ultrashort pump $I_s(t)$ onto a low bandgap material, electrons are promoted from the valence to the conduction band, switching its optical transmission on the timescale of the pump pulse. Typically, this drop of transmission occurs on a timescale of

Optics EXPRESS

a few tens of femtoseconds and acts as a semiconductor switch on the transmitted probe $P(t)$ [19], and remains for more than tens of picoseconds [20,21] (see Fig. 15 in the appendix). By measuring the transmitted spectrum of the probe as a function of the pump-probe delay τ, the resulting transient absorption spectrogram is described by :

$$I(\omega, \tau) = \left| \int_t P(t) S(t-\tau) e^{i\omega t} \mathrm{d}\, t \right|^2 . \tag{2}$$

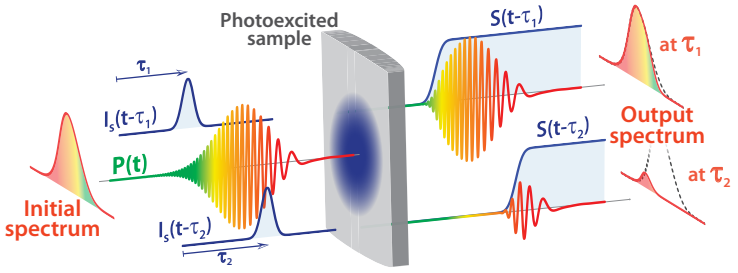

Fig. 1. Principle of the frequency resolved optical switching – The solid sample is photoexcited by a pump pulse $I_S(t)$ at variable pump-probe delays. Here, two different delays (τ_1 and τ_2) are illustrated. This acts as a transmission filter $S(t)$ for a probe pulse $P(t)$ (chirped in this the example) that changes its transmitted waveform and whose spectrum is measured.

The spectrogram is processed with a ptychographic algorithm (see appendix) allowing the retrieval of the temporal profiles of both the probe $P(t)$ and the optical switch $S(t)$.

In the measured spectrogram, the delay-dependent information of the optical switch $S(t)$ is encoded in the transmissivity drop, and that of the spectral phase of $P(t)$ is contained in the cut-off delay of each frequency. In the extreme case of a highly chirped probe pulse, the cut-off delay as a function of frequency directly maps the group delay. This particular case was observed for a highly chirped supercontinuum with a picosecond duration [22]. In addition, transient absorption in solids and plasmas was previously proposed to estimate [23] and measure sub-ps pulses [24].

Here, we combine the transient absorption approach with the strength of ptychography providing a powerful and robust method to retrieve the spectral phase of ultrashort pulses leading to complete temporal characterization.

It should be noted that Eq. (2) is identical to the equation describing FROG measurements [10]. Recently, ptychographic algorithms were adapted to reconstruct FROG spectrograms and led to so-called 'time-domain ptychography' [25,26]. A strong improvement in the reconstruction procedure was further demonstrated [27–29]. However, in all these time-domain ptychography studies to date, the reconstructed spectrograms result from conventional FROG measurements. In other words, while significant enhancement of the retrieval procedure is made using these algorithms, the nature of the measurement is unchanged, and these time-domain ptychography studies are computational improvements of FROG measurements. Here, the process at the core of the measurement is changed in order to eliminate the necessity of frequency conversion. The temporal profiles of the probe pulse $P(t)$ and of the optical switch $S(t)$ are extracted from the spectrogram with a ptychographic procedure, as described in the appendix.

3. Experimental setup

The experiments were carried out at the Advanced Laser Light Source (ALLS) laboratory. The measurement scheme for frequency resolved optical switching is illustrated in Fig. 2. A pump and a probe beam are focused on a thin solid sample. The pulse to be characterized (or probe

Optics EXPRESS

in the ptychographic procedure) is focused by an off-axis parabolic mirror. The pump pulse is focused through a hole in the parabola. The relative angle is 3° between both beams. The pump wavelength is chosen such that the pulse is absorbed at the surface of the sample. The focus of the pump beam is set a few-cm after the sample to excite the material on a large surface compared to the probe spot size. After the sample, the probe is re-imaged into a spectrometer. A delay line controls the delay (τ) between the pump and the probe. Different dispersive media can be introduced in the probe beam path in front of the focusing parabola in order to add group velocity dispersion to test the robustness of the technique by retrieving the dispersion of materials (see Fig. 5).

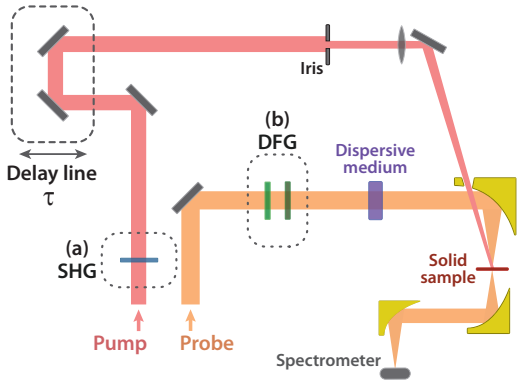

Fig. 2. Experimental setup – (a) – To characterize short pulses at 0.77 μm, the pump pulses at 0.4 μm are obtained by frequency doubling 0.8 μm-pulses in a BBO crystal followed by two dichroic mirrors to filter the remaining 0.8 μm. – (b) – To generate mid-IR pulses by difference frequency generation (DFG) between the signal and the idler at the output of an optical parametric amplifier (OPA), a nonlinear crystal is inserted together with a long pass filter that transmits only the DFG output (4 or 10 microns). – Different dispersive media are used to validate the technique (see Fig. 5).

We have characterized ultrashort pulses at five different central wavelengths, from the near-infrared to the mid-infrared, and with duration down to sub-two cycles. Here are the experimental details for pulse characterization in each spectral range.

3.1. Setup for the characterization of near-infrared pulses

The experimental scheme for the characterization of near-infrared pulses corresponds to Fig. 2(a). This experiment was performed on the ALLS kHz beamline delivering (for this case) 0.7 mJ 45 fs-pulses centered at 0.8 μm. The beam is divided in two arms by a 50-50 beam splitter. In the pump arm, the pulse is frequency doubled by a 1mm-thick Beta Barium Borate (BBO) crystal and the remaining 0.8 μm is filtered by two dichroic mirrors. It results in pulses with duration of 55 fs full width at half maximum (FWHM) in intensity centered at 0.4 μm (see TG FROG measurements of the pump pulses in the appendix - Fig. 13). These 50 μJ pulses are focused a few millimeters after the solid sample so that the beam diameter is ~200 μm on its surface. At this position, the fluence on the solid is evaluated to be 160 mJ/cm^2. As this fluence is above the ablation threshold, the sample is slightly moved out of focus to avoid ablation while keeping a high absorption contrast. In the probe arm, the beam of 350 μJ pulses is focused into a 2 m stretched hollow-core fiber filled with R152a with a differential pressure whose maximum is 620 torr [30]. The spectral broadening provides 6 fs Fourier-limited pulses centered at 0.77 μm with 220 μJ energy. Ten chirped mirrors whose group velocity dispersion (GVD) is −50 fs^2 per pair (total of −250 fs^2 GVD) together with two thin wedges (3° angle) are used to post-compress the

Optics EXPRESS

pulses. Pulses of 80 μJ are obtained with a duration of ~8 fs (characterized with a home-built SHG FROG for comparison with frequency resolved optical switching). Using the reflection of two wedges, the pulse energy is reduced to less than 10 nJ. An iris and an off-axis parabolic mirror (10 cm-focal length) are used to focus the beam with a spot diameter of 25 μm at the solid surface. Its fluence is estimated to less than 0.5 mJ/cm^2. The solid sample used for the measurements is a 500 μm-thick zinc selenide (ZnSe) plate that transmits the probe and absorbs the pump. The spectrometer measuring the probe spectrum is a HR4000 spectrometer from Ocean Optics.

3.2. Setup for the characterization of infrared pulses

The experimental scheme for the characterization of infrared pulses corresponds to Fig. 2. This experiment was performed on the 50 Hz high energy beamline in ALLS. Pulses of 20 mJ and 65 fs at 0.8 μm are delivered. For the pump pulses, a 90-10 beam splitter in the path of the 0.8 μm line selects 10% of the 20 mJ beam. Then, an iris selects a 5 mm-diameter beam with ~600 μJ energy per pulse which is focused a few centimeters after the solid sample. The pump diameter is larger than 500 μm and the fluence on sample is evaluated to 300 mJ/cm^2. As before, this is above the ablation threshold and the sample is slightly moved out of focus in order to avoid ablation while keeping a high absorption contrast. In the probe arm, an OPA (Light Conversion, TOPAS) converts 1.2 mJ into a 300 μJ signal and idler. The idler is then further amplified by a high energy OPA stage pumped by 18 mJ pulses at 0.8 μm. At the output, we obtain two co-propagating beams with orthogonal polarization centered at 1.53 and 1.75 μm, with a total energy of 4 mJ. They are 32.7 and 28.9 fs Fourier-transform limited, respectively. Either the 1.53 or 1.75 μm pulse is selected for characterization by blocking one arm of an interferometer (placed at the output of the OPA to control the relative delay between the signal and idler). The reflection from two wedges is reducing the energy down to less than 0.2 μJ. An iris and a 5 cm off-axis parabola are used to focus the beam to a spot with a diameter of 30 μm on the solid sample. Its fluence is estimated to be less than 1.5 mJ/cm^2.

The solid sample for the measurements is a 500 μm-thick silicon (Si) plate which transmits the signal and idler and absorbs the 0.8 μm pump. The spectrograms are acquired using a NIR256 spectrometer from Ocean Optics. To compare the frequency resolved optical switching technique, the pulses are also characterized with a home built SHG-FROG.

3.3. Setup for the characterization of mid-infrared pulses

The optical setup used to characterize the pulses at 1.53 and 1.75 μm was also used to measure pulses centered at 4 and 10 μm. The experimental scheme corresponds to Fig. 2(b). The pump arm is identical to the previous section.

For the 4 μm probe pulses, the OPA is tuned to generate 1.35 and 2 μm signal and idler pulses with a total energy of ~4 mJ. Pulses with 30 μJ at 4 μm are generated by difference frequency generation (DFG) in a 180 μm-thick $LiGaSe_2$ crystal. The pulses are 30.6 fs Fourier-transform limited. A 2 mm-diameter iris selects ~1 μJ per pulse and the beam is focused on a ~100 μm focal spot. The fluence on the solid is estimated to less than 10 mJ/cm^2. The different solid samples used are a 500 μm-thick Si sample and a 300 μm-thick germanium (Ge) sample. In addition, the 4 μm-pulses were also characterized with a 500 μm-thick ZnSe sample to compare the pulse reconstruction with different optical switches. In this case, the 0.8 μm pump pulses were frequency doubled in a 1 mm-thick BBO crystal. Two dichroic mirrors filter the remaining 0.8 μm. The whole beam of 500 μJ pulses is focused after the sample by 0.8 mm to set its diameter to 500 μm. The fluence on the solid is here estimated to be 200 mJ/cm^2. Above this fluence, we observe ablation of the ZnSe.

For the 10 μm probe pulses, the OPA is tuned to generate 1.53 and 1.75 μm signal and idler pulses with a total energy of ~4 mJ. 18 μJ pulses centered at 10 μm are generated by DFG in a

Optics EXPRESS

180 μm-thick GaSe crystal. The pulses are 43.6 fs Fourier-transform limited. A 3.5 mm-diameter iris selects ~1.5 μJ per pulse focused on a 300 μm-thick Ge plate with a ~140 μm focal spot. The fluence on the solid is estimated to less than 8 mJ/cm^2.

The spectrograms at 4 and 10 μm are measured using a spectrometer based on the CM110 monochromator from Spectral Products, with the HgCdTe (MCT) bolometric detector from Infrared Associates Inc. cooled with liquid nitrogen.

It is important to highlight that these measurements are a proof of principle of the frequency resolved optical switching technique, therefore, we took advantage of the rather high energy pump pulses that were available. This way the pump beam on the solid sample was far larger than the probe beam. Consequently, the alignment was an easy procedure, and the contrasts of the spectrograms were high and far above the measurement noise. However, these measurements could have been performed with pump pulses whose energy is much lower, as shown in Fig. 7.

4. Experimental results

In order to demonstrate the capability and robustness of the frequency resolved optical switching method, we have (i) characterized ultrashort pulses, with a duration down to sub-two cycles, for five central wavelengths: 0.77, 1.53, 1.75, 4, and 10 μm and compared to SHG FROG measurements for the case of 0.77, 1.53 and 1.75 μm; (ii) measured the dispersion introduced by a variety of known dispersive media between 0.6 and 14.5 μm and compared it to the dispersion predicted from Sellmeier equations of the different materials; (iii) demonstrated that the technique is independent of the optical switch by characterizing identical few-cycle pulses at 0.77 μm with two different switch durations, and at 4 μm with three different solids; (iv) and characterized ultrashort pulses from 1.75 to 9.5 μm using a single setup, i.e. the same pump pulses at constant fluence and the same material to induce the optical switch.

In all our experiments, the solid is photoexcited only near its surface on a sub-μm to 10 μm-scale by using pump pulses with a photon energy above the band gap. At 0.4 μm, the absorption coefficient for ZnSe is ~150000 cm^{-1} [31]. For Si and Ge at 0.8 μm, the absorption coefficients are ~850 cm^{-1} [32] and ~50000 cm^{-1} [33] respectively. In these cases, 80% of the pump energy is absorbed in the first 0.1, 18, and 0.3 μm at the surfaces of ZnSe, Si, and Ge respectively. This precaution avoids the contribution of both group velocity mismatch and group delay dispersion due to propagation in the solid. In addition, a uniform excitation of the solid is provided by setting the pump spot size significantly larger than that of the probe.

Figure 3 presents the frequency resolved optical switching measurements of the pulses centered at 0.77, 1.53 and 1.75 μm, and the comparison with the SHG FROG measurements. Note that the temporal phase of $S(t)$ is not shown here as it barely varies with time, but it can be found in the appendix. This confirms that the pumping of the solid samples acts mostly on their transmission as an amplitude non-stationary filter.

As can be observed by comparing the red and black curves on the right panels of Fig. 3, both the frequency resolved optical switching and SHG FROG measurements retrieve almost the same temporal structure. The ultrashort pulses at 0.77 μm, Fig. 3(a), have durations of 8.5 and 7.8 fs FWHM respectively measured by frequency resolved optical switching and SHG FROG. It should be noted that such a difference is typical for the characterization of few-cycle pulses. The pulse durations at 1.53 μm are measured to 41 or 40fs FWHM by frequency resolved optical switching or SHG FROG, and 37 or 34fs for the pulses at 1.75 μm.

Figure 4 presents the frequency resolved optical switching measurements of the pulses centered at 4 and 10 μm whose respective durations are 50 and 53fs FWHM. Note that at 10 μm, the duration corresponds to sub-two optical cycles with spectra spanning over more than one octave, from 6 to 14.5 μm.

To further validate the frequency resolved optical switching capability, the addition of spectral phases due to the linear propagation in different dispersive media with various thicknesses

Optics EXPRESS

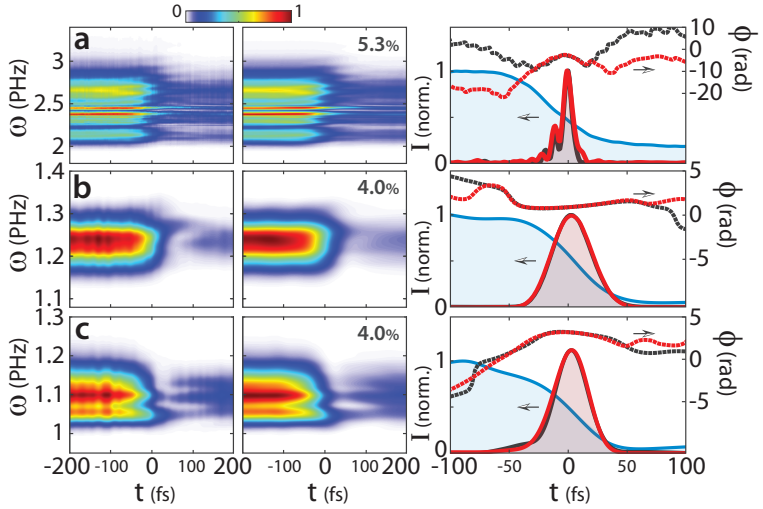

Fig. 3. Frequency resolved optical switching characterization of near-IR pulses – For pulses whose wavelengths are centered at (a) 0.77, (b) 1.53, and (c) 1.75 μm. Left panels, experimental spectrograms in intensity. Middle panels, reconstructed spectrograms with the reconstruction error as defined in the appendix, see Eq. (6). Right panels, in red, retrieved probe pulses $P(t)$ in intensity (solid line) and phase (dash line), in blue, retrieved switch profiles $S(t)$ in intensity, and in black, retrieved pulse profiles (intensity and phase) with SHG FROG measurements.

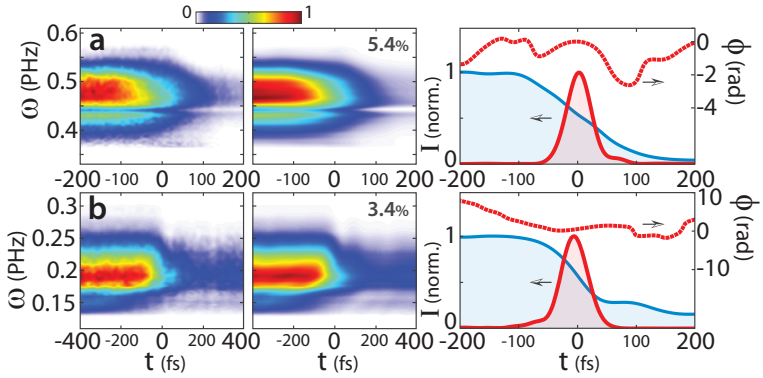

Fig. 4. Frequency resolved optical switching characterization of mid-IR pulses – For pulses whose wavelengths are centered at (a) 4, and (b) 10 μm. – Left panels, experimental spectrograms in intensity. – Middle panels, reconstructed spectrograms with the error factor as defined in the appendix. Right panels, in red, retrieved probe pulses $P(t)$ in intensity (solid line) and phase (dash line), and in blue, retrieved switch profiles $S(t)$ in intensity.

(see experimental scheme in Fig. 2) was characterized for the five spectral ranges of the pulses presented in Fig. 3 and 4. As shown in Fig. 5, the agreement with the phase shift calculated using the Sellmeier equations is excellent at all wavelengths and for all dispersive media. Furthermore, our technique is sensitive to the sign of the dispersion as demonstrated in Fig. 5(b).

To demonstrate the robustness of the technique, we compare the characterization of identical pulses by inducing the optical switch (**i**) with two different pump pulse durations, (**ii**) with different pump fluences, (**iii**) by pumping different solids, and (**iv**) by fixing the pump and

Optics EXPRESS

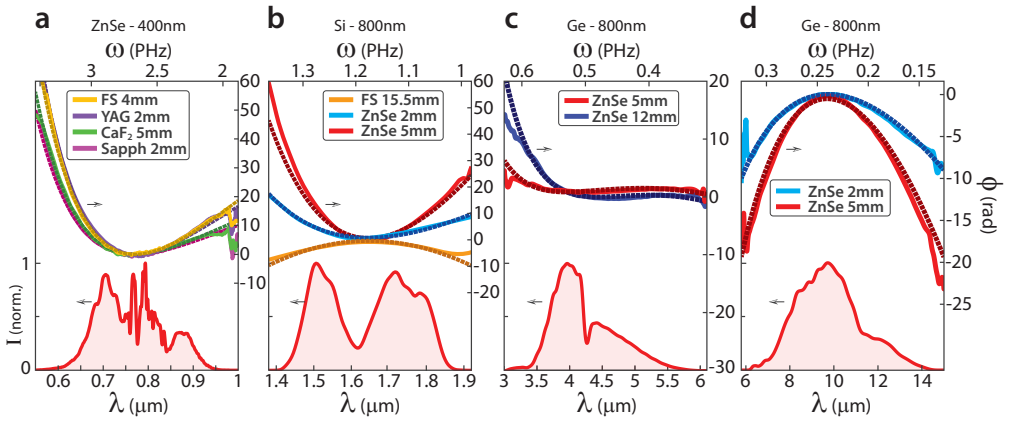

Fig. 5. Characterization of the dispersion of different materials – For pulses centered at 0.77 μm, panel (a), 1.53 and 1.75 μm (signal plus idler), (b), 4 μm, (c), and 10 μm, (d), the spectrum is shown at the bottom in red. – Dispersion of different materials, see legend, measured with frequency resolved optical switching, solid lines, and compared with the Sellmeier equations, dash lines. – The photoexcited material and the pump wavelength used to create the optical switch are mentioned at the top of the panels.

the solid but changing the central wavelength of the characterized pulses from 1.75 to 9.5 μm covering more than 3 octaves of spectral bandwidth.

(**i**) In Fig. 6, few-cycle pulses at 0.77 μm are characterized with two different switch durations created by pumping a ZnSe sample with 0.4 μm pulses. The pulses presented in panel (e) are almost identical, with pulse durations of 8.5 and 8.2 fs, while the optical switch profiles in panel (f) are different, as induced by pump pulse durations of 55 and 101 fs respectively (see TG FROG measurements of the pump pulses in the appendix - Fig. 13). The 101 fs pump pulses have been obtained by inserting fused silica in the beam path of the 55 fs pulses.

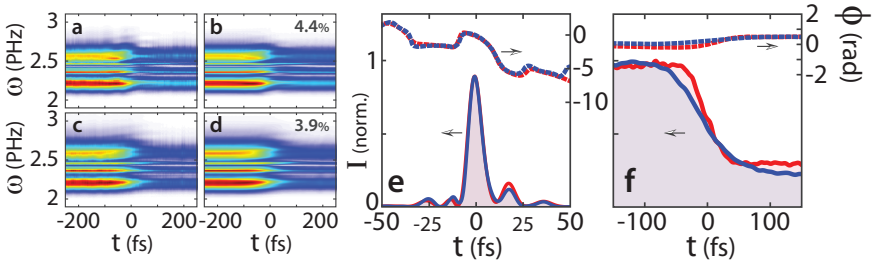

Fig. 6. Frequency resolved optical switching measurements of identical 0.77 μm-pulses with different pump pulse durations. – Switch parameters: ZnSe sample pumped with 0.4 μm pulses with 55fs (panels (a) and (b) and red lines on panels (e) and (f)) and 101fs duration (panels (c) and (d) and blue lines on panels (e) and (f)). – (a) to (d) – Measured and reconstructed spectrograms on the first and second columns. – (e)/(f) – Retrieved profiles, in intensity (solid lines) and phase (dashed lines), of 0.77 μm probe pulses $P(t)$, panel (e), and of the switches $S(t)$, panel (f).

(**ii**) In Fig. 7, pulses at 1.75 μm are characterized with photoexcited Si sample at different pump pulse fluences. The maximum fluence is close to the ablation threshold, evaluated to be lower than 300 mJ/cm^2 for 100% of the laser energy (see alignment procedure in the experimental setup section). The pump pulse energy is reduced down to 10% of this maximum. As can

Optics EXPRESS

be observed on panel (f), the retrieved profiles of the probe pulse are almost identical for all measurements except for the one with the lowest contrast (10% pump energy). Moreover, the normalized profiles (between 0 to 1) of the retrieved switch in panel (h) exhibit the same slope. These results demonstrate that the frequency resolved optical switching technique is valid as long as the spectrogram contrast is sufficient (near 25%). Under our experimental conditions, this was the case for a pump energy in the range of 150 to 600 μJ.

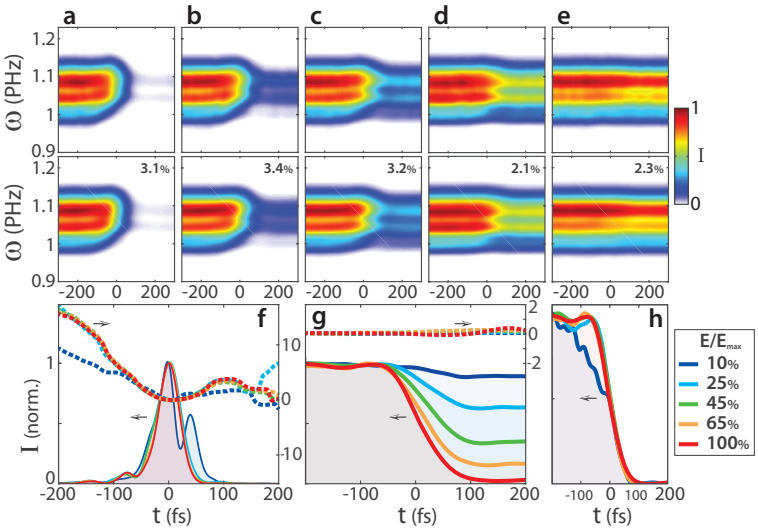

Fig. 7. Frequency resolved optical switching characterization of 1.75 μm pulses using different pump energies. – (a) to (e) – Measured and reconstructed traces for 0.8 μm pump pulses with respective energy of 10, 25, 45, 65, and 100% of 600 μJ, photoexciting a Si sample. – (f)/(g) – Retrieved profiles of the probe pulse and of the optical switch. – (h) – Normalized profiles of the optical switch (minimum at zero, maximum at one).

It is important to note that here, as pump pulses of hundreds of microjoules were available, the pump beam on the sample was set far larger than the probe one : more than 500 μm-diameter compared with 30 μm. If such a high energy is not available, the pump beam size can be adjusted to have a fluence of a few tens of millijoules per centimeter square for the spectrogram contrast to be above the measurement noise. For instance, here to keep the same pump fluence on sample (case 25% of Fig. 7), if the beam size is divided by a factor of two (to be 250 μm), its energy per pulse could be only 150/4 = 37.5 μJ to perform the same measurement.

(**iii**) In Fig. 8, pulses centered at 4 μm are measured using three different solids and two different pump wavelengths – Ge pumped at 0.8 μm, Si at 0.8 μm, and ZnSe at 0.4 μm. While the temporal profiles of the three optical switches are different, the retrieved pulses are almost identical, with durations of 51, 49, and 53 fs respectively.

(**iv**) In Fig. 9, pulses centered at 1.75, 4.5, and 9.5 μm are measured using Si pumped with a constant pump fluence (~240 mJ/cm^2) at 0.8 μm. Here, it is interesting to note that we retrieve almost the same temporal profile for the gate for each characterized central wavelength. It is important to note that all the measurements are performed over several hours and the laser has intrinsic fluctuations that could easily explain the minor differences between the retrieved optical switches.

The results obtained in Fig. 6, 7, 8, and 9 further confirm that under the conditions explored in this work, propagation in the solid does not play a significant role on frequency resolved optical switching.

Optics EXPRESS

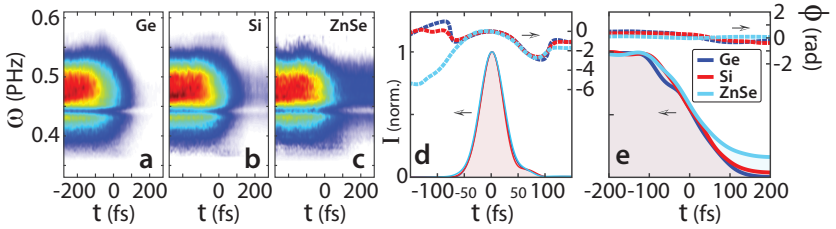

Fig. 8. Frequency resolved optical switching measurements of identical 4 μm-pulses with different switch materials. – (a)/(c) – Measured spectrograms of the 4 μm-probe pulses obtained by pumping a sample of Ge at 0.8 μm, panel (a), of Si at 0.8 μm, panel (b), and ZnSe at 0.4 μm, panel (c). – (d)/(e) – Retrieved profiles, in intensity (solid lines) and phase (dashed lines), of probe pulses $P(t)$, panel (d), and of the switches $S(t)$, panel (e). Colors: see legend in panel (e).

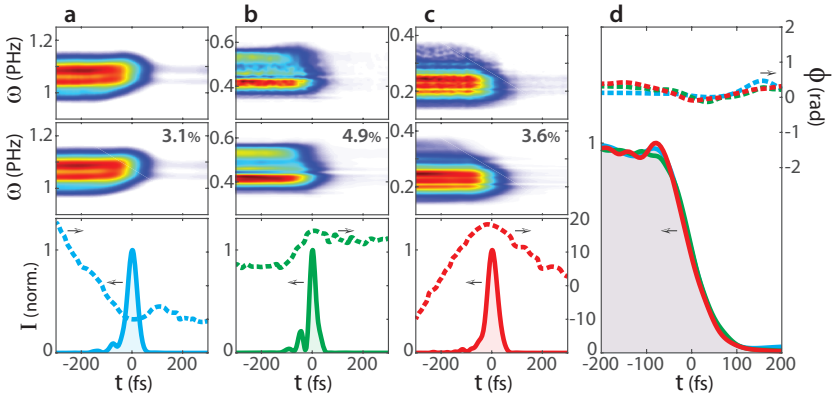

Fig. 9. Frequency resolved optical switching characterization with different pulses with a single setup – (a)/(b)/(c) – Measured and reconstructed spectrograms, and retrieved pulse profiles, for pulses centered at 1.75 (blue), 4.5 (green), and 9.5 μm (red). – (d) – Retrieved profiles of the optical switch (corresponding colors of the panels (a) to (c)).

5. Conclusion

We introduce the frequency resolved optical switching technique capable of measuring femtosecond pulses from the visible to the mid-IR spectral range. Using transient absorption in solids, an ultrafast optical switch is generated to characterize ultrashort pulses. The temporal profiles of both the switch and the pulse are retrieved from the spectrogram with a ptychographic algorithm. To demonstrate the strength of this approach, that is free of phase-matching, ultrashort pulses centered at 0.77, 1.53, 1.75, 4, and 10 μm were measured, with sub-two cycle duration for the latter. The technique, cross-checked with FROG measurements, was proven to be robust against changes in the optical switch. Note that this technique is easy to implement and enables the characterization of ultrashort pulses from the near to mid-IR spectral range.

As the spectral limitation of this metrology is given by the optical transmissivity of the solid, pulses with a spectrum extending from the visible to the mid-IR, either tunable or continuous, can be characterized. For instance, ZnSe is transparent from ~0.5 to 20 μm and can be pumped at 0.4 μm as demonstrated in this paper. In most cases, these pulses are obtained from an OPA pumped at a short wavelength, providing the pump pulses required for photoexcitation in the frequency resolved optical switching procedure. Thus, this technique is particularly convenient

Optics EXPRESS

to characterize OPA output pulses as well as their extension to the long wavelength range via nonlinear processes [1,34].

The other limitation of this technique is the requirement of an intense pulse for the pump beam. Here, pump pulses of a few hundred microjoules were available and used to demonstrate a proof of concept. As mentioned previously, the pump beam can be focused more tightly on the sample thus enabling measurements with a few tens of microjoules for the pump pulses.

We characterized pulses with spectra extending from 0.6 to 5 μm with ZnSe, 3 to 15 μm with Ge, and 1.4 to 14.5 μm with Si. Therefore, with such a device, many pulses generated in a laser laboratory can be measured with a single optical setup, as demonstrated by Fig. 9. As a perspective, this technique paves the way to temporally characterize pulses at the frontier of current technologies, covering multi-octaves of spectral bandwidth even at nJ energy levels, which remains extremely challenging by any other means.

6. Appendix

6.1. *Frequency resolved optical switching characterization of pulses in the spectral range from 0.6 to 15 μm*

Figure 10 shows the reconstructed profiles of the measurements illustrated in Fig. 3 and 4 of the main text for the characterization of pulses centered at 0.77, column (a), 1.53, (b), 4, (c), and 10 micrometers, (d). The first and second rows show the retrieved temporal profiles of the probe pulse $P(t)$ and the switch $S(t)$ (in intensity and phase). Superimposed with thin blue lines are the retrieved profiles from multiple independent reconstructions – 5 for panels (a) to (c) and 10 for panels (d). The final reconstructions correspond to the average of the multiple reconstructions, and are shown with thick red lines (for more information, see the appendix section called "The reconstruction procedure").

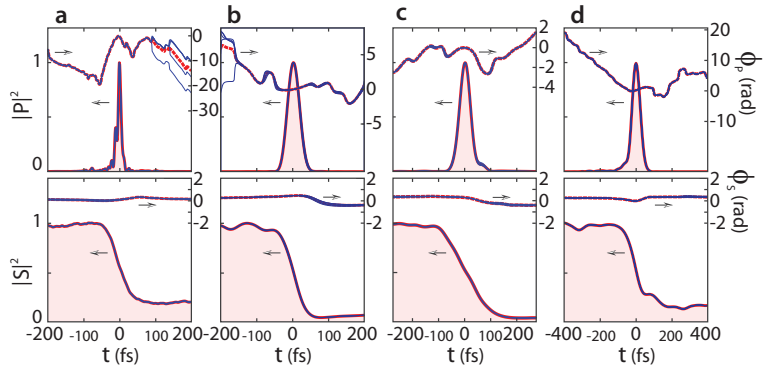

Fig. 10. Frequency resolved optical switching characterization of various pulses – Retrieved profiles of the probe pulses (top panels) and of the switch (low panels) for different independent reconstructions in blue lines, and the average one in red lines. – (a) – Few-cycle pulses centered at 077 μm, duration 8.5 fs FWHM, corresponding to the measurement of Fig. 3(a) . – (b) – 40 fs-pulses centered at 1.53 μm, corresponding to the measurement of Fig. 3(b). – (c) – 50 fs-pulses centered at 4 μm, corresponding to the measurement of Fig. 4(a). – (d) – Few-cycle pulses centered at 10 μm, duration 53fs, corresponding to the measurement of Fig. 4(b).

6.2. *SHG FROG characterization of the probe pulses at 0.77, 1.53, and 1.75 μm*

To compare the frequency resolved optical switching technique with a conventional characterization technique, the pulses centered at 0.77, 1.53, and 1.75 μm of Fig. 3 of the main text are

Optics EXPRESS

characterized by SHG FROG with a 10 μm-thick BBO crystal, as illustrated in Fig. 11. These SHG FROG reconstructions are superimposed with those from the frequency resolved optical switching in the right panels of Fig. 3 of the main text.

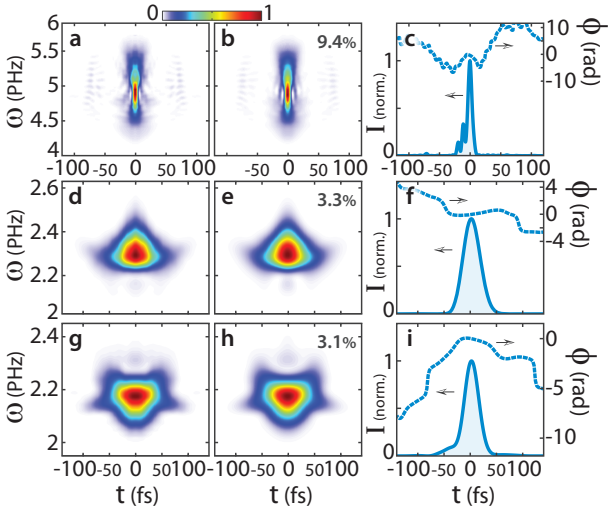

Fig. 11. SHG FROG characterization of pulses centered at 0.77, 1.53 and 1.75 μm – Characterization of pulses centered at 0.77 μm, first row, at 1.53 μm, second row, and at 1.75 μm, third row. – SHG FROG spectrograms measured, first column, and reconstructed, second column. Retrieved pulse temporal profiles in intensity and phase, last column.

6.3. *SHG FROG characterization of the pump pulses at 0.8 μm*

For the frequency resolved optical switching measurements of the pulses centered at 1.53, 1.75, 4, and 10 μm, the same pump pulse centered at 0.8 μm was used. This pump pulse was characterized by SHG FROG as presented in Fig. 12. The pulse duration is 65fs FWHM in intensity.

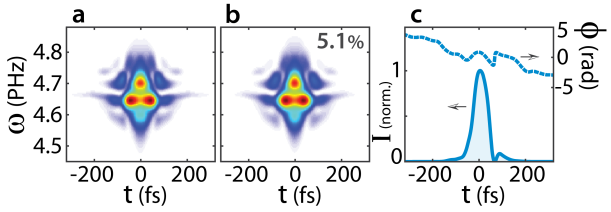

Fig. 12. SHG FROG characterization of the pump pulse centered at 0.8 μm – Measured and reconstructed SHG FROG spectrograms on panels (a) and (b) – Retrieved profile of the pump pulse intensity (solid line) and phase (dash line).

6.4. *Testing the independence from the switch function*

In order to test the robustness of the frequency resolved optical switching technique, identical pulses centered at 0.77 and 4 μm were characterized with different switches, see Fig. 6 and 8 of the main text.

Optics EXPRESS

6.4.1. TG FROG characterization of the 0.4 μm pump pulses

Pulses whose durations are 8 fs and centered at 0.77 μm were characterized with switches induced by pump pulses with two different durations. This was made by stretching the pump pulse duration at 0.4 μm from 55 fs to 101 fs with a 10 mm-thick fused silica window. The pump pulses are measured by TG FROG as illustrated in Fig. 13.

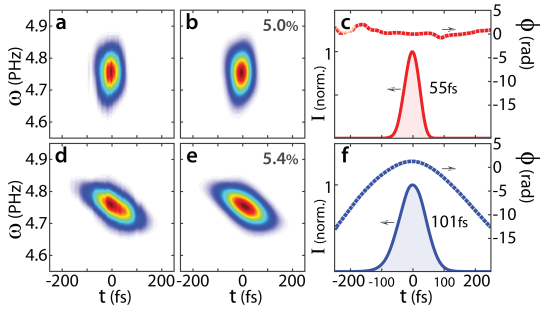

Fig. 13. TG FROG characterization of the pump pulses centered at 0.4μm – On the second row, the pulse of the first row is chirped by a 10 mm-thick fused silica window. – TG FROG spectrograms measured, first column, and reconstructed, second column. – Reconstructed pulses in intensity and phase, last column.

6.4.2. Pulse characterization of the 4 μm pulses with different photoexcited materials

For identical 4 μm-probe pulses, three frequency resolved optical switching measurements are recorded by using samples of Ge (300 μm thick) and Si (500 μm thick) pumped with 0.8 μm pulses and of ZnSe (500 μm thick) pumped with 0.4 μm pulses, see Fig. 14. The retrieved temporal profiles of the pulses $P(t)$ and the switch $S(t)$ are superimposed in Fig. 8(d) and (e) of the main text.

6.5. *Transmission of the photoexcited Si sample up to 80ps pump-probe delay*

Figure 15 presents the measured transmission of the Si sample, pumped at 0.8 μm (fluence close to the ablation threshold) and probed at 4 μm, up to 80 ps delay after the photoexcitation. The transmission drops by more than 90% at 0 delay, and remains low for several tens of ps.

6.6. *Reconstruction procedure*

6.6.1. Retrieval algorithm

The phase retrieval procedure aims to retrieve the temporal functions of the pulse $P(t)$ and switch $S(t)$ of Eq. (2) of the main text, which better describe the experimental spectrogram. We use a ptychographic phase retrieval algorithm that is usually applied to spatial measurements [18,35]. For this temporal scheme, the probe and object in ptychography correspond to the pulse and the switch.

Defining $Q(t,\ t_0) = P(t)S(t-t_0)$ as the product of the pulse and switch functions delayed by t_0, Eq. (2) can be rewritten in :

$$I(\omega, t_0) = \left|\mathcal{F}\left[Q(t,\ t_0)\right]\right|^2 , \tag{3}$$

where $\mathcal{F}$ and $\mathcal{F}^{-1}$ are the direct and inverse Fourier transform respectively from time domain to frequency domain $t \rightarrow \omega$ or opposite $\omega \rightarrow t$.

The reconstruction strategy consists of combining two projections, either in the temporal or frequency domain, to iteratively update $Q(t,\ t_0)$.

Optics EXPRESS

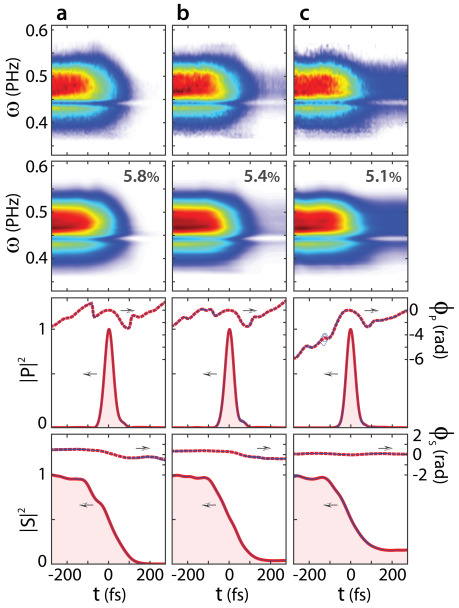

Fig. 14. Frequency resolved optical switching characterization of identical 4 μm-pulses with different solid samples – For a sample of Ge, column (a), Si, (b), and ZnSe, (c) : first and second rows, measured and reconstructed spectrograms; third and last rows, retrieved pulse and switch temporal profiles in intensity and phase.

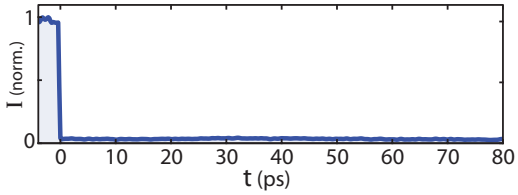

Fig. 15. Transmission of the photoexcited Si sample up to 80ps pump-probe delay. – Transmission of the Si sample pumped at 0.8 μm, probed at 4 μm.

- In the frequency domain, the *experimental projection* Π_{XP} aims at constraining the Fourier magnitude of Q to the measured spectrogram $I_{XP}(\omega, t_0)$. It can be mathematically written as:

$$\Pi_{XP}\left[Q(t,\ t_0)\right] = \mathcal{F}^{-1}\left[\frac{\mathcal{F}\left[Q(t,\ t_0)\right]}{\left|\mathcal{F}\left[Q(t,\ t_0)\right]\right|}\sqrt{I_{XP}(\omega, t_0)}\right]. \tag{4}$$

- The second projection, termed here the *product projection*, consists of fitting $Q(t,\ t_0)$ by a product of two functions.

$$\Pi_{prod}\left[Q(t,\ t_0)\right] = P_g(t)S_g(t - t_0)\,, \tag{5}$$

where the two guessed functions $P_g(t)$ and $S_g(t)$ are obtained by minimizing the least-square error given by:

$$\epsilon = \sum_{t,t_0}\left|Q(t,\ t_0) - P_g(t)S_g(t - t_0)\right|^2. \tag{6}$$

Optics EXPRESS

It is at minimum if the (complex) gradient of ϵ with respect to P_g and to S_g are both equal to 0 : $\partial\epsilon/\partial P_g = \partial\epsilon/\partial S_g = 0$, which gives the following set of equations :

$$P_g(t) = \frac{\int Q(t,\ t_0) \cdot S_g^*(t - t_0)dt_0}{\int |S_g(t_0)|^2 dt_0} , \tag{7}$$

$$S_g(t) = \frac{\int Q(t + t_0,\ t_0) \cdot P_g^*(t + t_0)dt_0}{\int |P_g(t + t_0)|^2 dt_0} . \tag{8}$$

This system can be numerically solved by iterations starting from a random complex function S_g. Then, P_g is estimated by Eq. (7), and S_g re-evaluated by Eq. (8). Repeating this procedure approaches the solution very rapidly (less than 10 iterations).

These two projections can be combined in different ways, exhibiting different converging behaviors to retrieve the two functions $P(t)$ and $S(t)$ that satisfy the two constraints : $Q_{(n+1)} = \Pi_{prod}\left[Q_{(n)}\right] = \Pi_{XP}\left[Q_{(n)}\right] = Q_{(n)}$. Here, two types of combination are used. The *Error Reduction* (ER) scheme [35] can be described mathematically, at iteration n, by:

$$Q^{ER}_{(n+1)} = \Pi_{XP}\left[\Pi_{prod}\left[Q_{(n)}\right]\right] , \tag{9}$$

and the *Hybrid Input-Output* (HIO) scheme [35] (that is a particular case of the *difference map* scheme [36]) by:

$$Q^{HIO}_{(n+1)} = Q_{(n)} + \Pi_{XP}\left[2\Pi_{prod}\left[Q_{(n)}\right] - Q_{(n)}\right] - \Pi_{prod}\left[Q_{(n)}\right] . \tag{10}$$

The accuracy of the reconstruction is evaluated by an error factor (or R-factor) that is defined by calculating the difference between the reconstructed spectrogram to the experimental one [18]:

$$Err = \sqrt{1 - \frac{\left|\iint \mathcal{F}\left[Q(t,\ t_0)\right] \cdot I_{XP}(\omega, t_0)d\omega dt_0\right|^2}{\iint \left|\mathcal{F}\left[Q(t,\ t_0)\right]\right|^2 d\omega dt_0 \cdot \iint \left|I_{XP}(\omega, t_0)\right|^2 d\omega dt_0}} . \tag{11}$$

Each algorithmic scheme exhibits a different converging behavior [35]. The ER slowly converges to the closest local solution to the initial guess as the error factor can only decrease from one iteration to the other. The HIO rapidly converges to a steady-state regime where it keeps exploring an area where all possible approximate solutions lie. In general, due to noise in the measurements it does not converge to one particular solution. It is practical to drop to an approximated solution after a few iterations, but not to converge to a local optimum as the error factor is not optimized.

6.6.2. Application to the measured spectrograms

The retrieval procedure to reconstruct the experimental spectrograms is applied as described:

- At iteration step $n = 0$, an initial delayed product is calculated with two random complex functions for the pulse and switch :

$$Q_{(0)}(t, t_0) = P_{rand}(t)S_{rand}(t - t_0) .$$

- The HIO algorithm is applied for the first 15 iteration steps to drop rapidly to an approximated solution. Then the ER algorithm is used to optimize the local solution.

Optics EXPRESS

- To optimize the converging behavior of the algorithm, as the switch is expected to be mostly an intensity function, the switch phase is set to zero for the first two thirds of the iteration steps. This corresponds to only considering the module of the guessed switch $|S_g|$ in Eq. (8). Finally for the last third of the iterations, this constraint is released. As shown in Fig. 16, releasing this constraint barely improves the reconstruction accuracy which confirms the switch mostly acts as an intensity filter.

  Other reconstructions were made without this constraint for the first two thirds of the iterations and the same pulse and switch functions were retrieved but after many more iteration steps, further confirming the switch is mostly an intensity filter. This procedure is used here only to accelerate the algorithm convergence.

- Each experimental spectrogram is reconstructed multiple times starting from different random functions at iteration step $n = 0$. For all reconstructions, the initial guess at step $n = 0$ and the first guess of S_g in Eq. (7) (for the Π_{prod} projection) at each iterative step n are random and different. Therefore, all reconstructions are totally independent at each of their steps. The final considered reconstruction results from the average of all the independent ones.

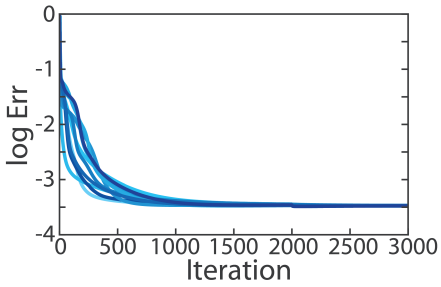

Fig. 16. Reconstruction error, defined by Eq. (11), as a function of the iteration step for ten independent reconstructions, see Fig. 10(d), of the spectrogram illustrated in the first panel of Fig. 4(b).

Figure 16 shows the reconstruction error, defined by Eq. (11), with the iteration step for the ten independent reconstructions superimposed in Fig. 10(d) (two lower panels). The experimental and reconstructed spectrograms are on the two higher panels.

Funding

H2020 Marie Skłodowska-Curie Actions (798205); Banting Research Foundation (201709BPF-393834-285459).

Acknowledgments

A. Leblanc acknowledges funding from the European Union's Horizon 2020 research and innovation programme under the Marie Skłodowska-Curie Grant Agreement No. 798205 and from the Canadian Banting Research Foundation No. 201709BPF-393834-285459. E. Haddad also acknowledges financial support from NSERC and FRQNT M. Sc. scholarship programs.

References

1. D. Sanchez, M. Hemmer, M. Baudisch, S. Cousin, K. Zawilski, P. Schunemann, O. Chalus, C. Simon-Boisson, and J. Biegert, "7 μm, ultrafast, sub-millijoule-level mid-infrared optical parametric chirped pulse amplifier pumped at 2 μm," Optica **3**(2), 147–150 (2016).

Optics EXPRESS

2. L. von Grafenstein, M. Bock, D. Ueberschaer, K. Zawilski, P. Schunemann, U. Griebner, and T. Elsaesser, "5 μm few-cycle pulses with multi-gigawatt peak power at a 1 kHz repetition rate," Opt. Lett. **42**(19), 3796–3799 (2017).
3. M. Bradler and E. Riedle, "Sub-20 fs μJ-energy pulses tunable down to the near-UV from a 1 MHz Yb-fiber laser system," Opt. Lett. **39**(9), 2588–2591 (2014).
4. T. Fuji and T. Suzuki, "Generation of sub-two-cycle mid-infrared pulses by four-wave mixing through filamentation in air," Opt. Lett. **32**(22), 3330–3332 (2007).
5. A. Wirth, M. T. Hassan, I. Grguraš, J. Gagnon, A. Moulet, T. T. Luu, S. Pabst, R. Santra, Z. A. Alahmed, A. M. Azzeer, V. S. Yakovlev, V. Pervak, F. Krausz, and E. Goulielmakis, "Synthesized Light Transients," Science **334**(6053), 195–200 (2011).
6. A. V. Mitrofanov, A. A. Voronin, D. A. Sidorov-Biryukov, S. I. Mitryukovsky, A. B. Fedotov, E. E. Serebryannikov, D. V. Meshchankin, V. Shumakova, S. Ališauskas, A. Pugžlys, V. Ya. Panchenko, A. Baltuška, and A. M. Zheltikov, "Subterawatt few-cycle mid-infrared pulses from a single filament," Optica **3**(3), 299–302 (2016).
7. D. Kartashov, S. Ališauskas, A. Pugžlys, A. Voronin, A. Zheltikov, M. Petrarca, P. Béjot, J. Kasparian, J.-P. Wolf, and Andrius Baltuška, "White light generation over three octaves by femtosecond filament at 3.9 μm in argon," Opt. Lett. **37**(16), 3456–3458 (2012).
8. C. Iaconis and I. A. Walmsley, "Spectral phase interferometry for direct electric-field reconstruction of ultrashort optical pulses," Opt. Lett. **23**(10), 792–794 (1998).
9. M. Anderson, A. Monmayrant, S.-P. Gorza, P. Wasylczyk, and I. Walmsley, "SPIDER: A decade of measuring ultrashort pulses," Laser Phys. Lett. **5**(4), 259–266 (2008).
10. K. W. DeLong, R. Trebino, and D. J. Kane, "Comparison of ultrashort-pulse frequency-resolved-optical-gating traces for three common beam geometries," J. Opt. Soc. Am. B **11**(9), 1595–1608 (1994).
11. R. Trebino, *Frequency-Resolved Optical Gating: The Measurement of Ultrashort Laser Pulses* (Springer Science & Business Media, 2012).
12. I. A. Walmsley and C. Dorrer, "Characterization of ultrashort electromagnetic pulses," Adv. Opt. Photonics **1**(2), 308–437 (2009).
13. J. N. Sweetser, D. N. Fittinghoff, and R. Trebino, "Transient-grating frequency-resolved optical gating," Opt. Lett. **22**(8), 519–521 (1997).
14. S.-W. Huang, G. Cirmi, J. Moses, K.-H. Hong, S. Bhardwaj, J. R. Birge, L.-J. Chen, E. Li, B. J. Eggleton, G. Cerullo, and F. X. Kartner, "High-energy pulse synthesis with sub-cycle waveform control for strong-field physics," Nat. Photonics **5**(8), 475–479 (2011).
15. M. Canhota, F. Silva, R. Weigand, and H. M. Crespo, "Inline self-diffraction dispersion-scan of over octave-spanning pulses in the single-cycle regime," Opt. Lett. **42**(15), 3048–3051 (2017).
16. S. B. Park, K. Kim, W. Cho, S. I. Hwang, I. Ivanov, C. H. Nam, and K. T. Kim, "Direct sampling of a light wave in air," Optica **5**(4), 402–408 (2018).
17. S. Keiber, S. Sederberg, A. Schwarz, M. Trubetskov, V. Pervak, F. Krausz, and N. Karpowicz, "Electro-optic sampling of near-infrared waveforms," Nat. Photonics **10**(3), 159–162 (2016).
18. P. Thibault, M. Dierolf, O. Bunk, A. Menzel, and F. Pfeiffer, "Probe retrieval in ptychographic coherent diffractive imaging," Ultramicroscopy **109**(4), 338–343 (2009).
19. C. Rolland and P. B. Corkum, "Generation of 130-fsec midinfrared pulses," J. Opt. Soc. Am. B **3**(12), 1625–1629 (1986).
20. M. Tyagi and R. Van Overstraeten, "Minority carrier recombination in heavily-doped silicon," Solid-State Electron. **26**(6), 577–597 (1983).
21. H. Němec, L. Fekete, F. Kadlec, P. Kužel, M. Martin, J. Mangeney, J. Delagnes, and P. Mounaix, "Ultrafast carrier dynamics in Br+-bombarded InP studied by time-resolved terahertz spectroscopy," Phys. Rev. B **78**(23), 235206 (2008).
22. F. Cilento, C. Giannetti, G. Ferrini, S. Dal Conte, T. Sala, G. Coslovich, M. Rini, A. Cavalleri, and F. Parmigiani, "Ultrafast insulator-to-metal phase transition as a switch to measure the spectrogram of a supercontinuum light pulse," Appl. Phys. Lett. **96**(2), 021102 (2010).
23. P. Hamm, C. Lauterwasser, and W. Zinth, "Generation of tunable subpicosecond light pulses in the midinfrared between 4.5 and 11.5 μm," Opt. Lett. **18**(22), 1943–1945 (1993).
24. K. Michelmann, U. Wagner, T. Feurer, U. Teubner, E. Förster, and R. Sauerbrey, "Measurement of the Page function of an ultrashort laser pulse," Opt. Commun. **198**(1-3), 163–170 (2001).
25. D. Spangenberg, P. Neethling, E. Rohwer, M. H. Brügmann, and T. Feurer, "Time-domain ptychography," Phys. Rev. A **91**(2), 021803 (2015).
26. T. Witting, D. Greening, D. Walke, P. Matia-Hernando, T. Barillot, J. Marangos, and J. Tisch, "Time-domain ptychography of over-octave-spanning laser pulses in the single-cycle regime," Opt. Lett. **41**(18), 4218–4221 (2016).
27. A. M. Heidt, D.-M. Spangenberg, M. Brügmann, E. G. Rohwer, and T. Feurer, "Improved retrieval of complex supercontinuum pulses from XFROG traces using a ptychographic algorithm," Opt. Lett. **41**(21), 4903–4906 (2016).
28. P. Sidorenko, O. Lahav, Z. Avnat, and O. Cohen, "Ptychographic reconstruction algorithm for frequency-resolved optical gating: super-resolution and supreme robustness," Optica **3**(12), 1320–1330 (2016).
29. T. Zahavy, A. Dikopoltsev, D. Moss, G. I. Haham, O. Cohen, S. Mannor, and M. Segev, "Deep learning reconstruction of ultrashort pulses," Optica **5**(5), 666–673 (2018).

Optics EXPRESS

30. E. Haddad, R. Safaei, A. Leblanc, R. Piccoli, Y.-G. Jeong, H. Ibrahim, B. E. Schmidt, R. Morandotti, L. Razzari, F. Légaré, and P. Lassonde, "Molecular gases for pulse compression in hollow core fibers," Opt. Express **26**(19), 25426–25436 (2018).
31. J. Salfi, U. Philipose, C. De Sousa, S. Aouba, and H. Ruda, "Electrical properties of Ohmic contacts to ZnSe nanowires and their application to nanowire-based photodetection," Appl. Phys. Lett. **89**(26), 261112 (2006).
32. M. A. Green, "Self-consistent optical parameters of intrinsic silicon at 300 K including temperature coefficients," Sol. Energy Mater. Sol. Cells **92**(11), 1305–1310 (2008).
33. W. Dash and R. Newman, "Intrinsic optical absorption in single-crystal germanium and silicon at 77 K and 300 K," Phys. Rev. **99**(4), 1151–1155 (1955).
34. M. Seidel, X. Xiao, S. A. Hussain, G. Arisholm, A. Hartung, K. T. Zawilski, P. G. Schunemann, F. Habel, M. Trubetskov, V. Pervak, O. Pronin, and F. Krausz, "Multi-watt, multi-octave, mid-infrared femtosecond source," Sci. Adv. **4**(4), eaaq1526 (2018).
35. J. R. Fienup, "Phase retrieval algorithms: a comparison," Appl. Opt. **21**(15), 2758–2769 (1982).
36. V. Elser, "Phase retrieval by iterated projections," J. Opt. Soc. Am. A **20**(1), 40–55 (2003).